

All-Dry Self-Adhesive Soft Electrodes with Subsurface Pores for Long-Term Skin Recording

Min Soo Jeon, Jonghun Yi, Seokkyoon Hong, Junsang Lee, Hanmin Jang, Bongjoong Kim, Haeyeon Lee, Chi Hwan Lee,* and Dong Rip Kim*

Long-term electrophysiological recording remains challenging, particularly on delicate skin, due to reliance on adhesive backings and conductive gels. Here, a class of all-dry, self-adhesive epidermal electrodes is presented by integrating low-density, octopus-like microstructures with porous subsurface architectures. This design offers key advantages, including low electrode-skin impedance, high air permeability, dynamic adhesion to prevent interfacial delamination, and mild adhesion strength for safe-and-easy removal. The electrodes enable stable, high-quality recordings over 24 h, maintaining signal integrity even under repeated skin deformation. Preclinical studies in healthy subjects demonstrate effective electrophysiological monitoring near the wrist and eye for > 24 h, highlighting potential applications in long-term, non-invasive monitoring scenarios such as neonatal intensive care unit monitoring, home healthcare, and sleep studies.

M. S. Jeon, J. Yi, J. Lee, H. Jang, H. Lee, D. R. Kim School of Mechanical Engineering Hanyang University Seoul 04763, Republic of Korea E-mail: dongrip@hanyang.ac.kr

S. Hong, J. Lee, B. Kim, C. H. Lee

Weldon School of Biomedical Engineering

Purdue University

West Lafayette, IN 47907, USA E-mail: lee2270@purdue.edu

B. Kim

 $Department \ of \ Mechanical \ and \ System \ Design \ Engineering$

Hongik University

Seoul 04066, Republic of Korea

C. H. Lee

School of Mechanical Engineering

Purdue University

West Lafayette, IN 47907, USA

C. H. Lee

Department of Materials Engineering

Purdue University

West Lafayette, IN 47907, USA

C. H. Lee

Elmore Family School of Electrical and Computer Engineering Purdue University

NV--+1-f---++- IN 4

West Lafayette, IN 47907, USA



The ORCID identification number(s) for the author(s) of this article can be found under https://doi.org/10.1002/smll.202507416

DOI: 10.1002/smll.202507416

1. Introduction

Repeated application and removal of epidermal electrodes over a prolonged period can weaken the skin barrier function, inducing pain, irritation, and delayed wound healing.[1-4] Long-term, real-time electrophysiological recording by an epidermal electrode is of importance in health monitoring and clinical cares.[5-8] Particularly, patients who have delicate skin due to immature and aging can greatly benefit from those technological advances.[9-11] Successful implementation of the epidermal electrode for long-term, real-time electrophysiological recording over delicate skin requires: 1) low-modulus suitable to skins for accurate recording, 2) proper breathability for mitigating inflammation, 3) sufficient adhesion for preventing delamination under dynamic human

motion, and 4) noninvasive skin interfacial adhesive for protecting delicate skin. To engage in those issues arising from delicate skin, a novel epidermal electrode platform has been successfully developed, including skin-level, low-modulus hydrogels and hydrogel-elastomer composites, [12-15] breathable holey device architectures, [16,17] microfluidic channel-embedded epidermal electrodes, [17-19] temperature-responsive epidermal electrodes. [20,21] Despite these promising demonstrations, many epidermal electrodes still rely on additional hydrogel-based skin interfacial adhesives for real-time electrophysiological recording, which may encounter signal degradation over time due to dehydration. It necessitates the development of all-dry epidermal electrode with no additional skin interfacial materials.

Dry epidermal electrode, in which electrically-conductive materials are directly contacted with skin, has attracted much attention as a candidate of long-term electrophysiological monitoring platforms to overcome dehydration of hydrogel-based wet epidermal electrode. In order to accomplish suitable mechanical compliance and breathability of dry epidermal electrodes, diverse configurations have been suggested, which include metal nanowire-polymer nanofiber networks,^[22,23] metallogel fiber networks,^[24] soft elastomer membrane with a conductive metal layer,^[25-27] porous graphene or metal nanowire and elastomer composites,^[28,29] and sub-micron ultra-thin conductive film.^[30,31] When pores or metal layers exist in the contacting surface of dry epidermal electrodes, skin interfacial adhesion greatly decreases,

16136829, D. Dowlookaded from https://onlinibithary.wiley.com/oi/01/01/02/smll.2029/146 by Chi Hwan Lee - Purtuse University (West Lafayetet), Wiley Online Library on [261012025]. See the Terms and Conditions (https://onlinelibitrary.wiley.com/terms-and-conditions) on Wiley Online Library for rules of use; OA articles are governed by the applicable Creative Commons Licensea

www.small-journal.com

which can lead to signal degradation by partial delamination in repeated skin deformation. [17,18,32,33] Forming the amphibianand octopus-like microscale structures on the contacting surfaces of dry epidermal electrodes may be a solution to increase skin interfacial adhesion, [34–37] but the robust bonding with delicate skin can result in iatrogenic skin injuries during removal. [17–20,38] The successful development of dry epidermal electrodes for delicate skin faces the challenges of resolving these contradictory constraints.

Herein, we demonstrate all-dry epidermal electrodes made with a carbon-doped silicone elastomer to enable safe-and-easy removal from delicate skin, while securing dynamic adhesion (i.e., the ability to maintain conformal contact with human skin during motion) with no additional modifications on skin interfacial adhesion. Specifically, to address the challenge in balancing the trade-off between strong adhesion for stable signal acquisition and weak adhesion for easy removal, all-dry epidermal electrodes are designed with reasonably low adhesion to enable easy removal, while maintaining long-term signal quality under deformation. This functionality is achieved by incorporating subsurface pores (i.e., pores located beneath the skin-contact surface) into the all-dry epidermal electrode, which serves to prevent delamination. It should be noted that excessively low adhesion can hinder initial attachment to the skin, and to address this, low-density, octopus-like microstructures are introduced on the bottom surface of the all-dry epidermal electrode to achieve a reasonable level of low adhesion. The all-dry epidermal electrode platform (hereinafter, referred as S-porous) can offer four representative features: 1) soft skincomparable, low-modulus (16-19 kPa) by the pore networks within the conductive electrode for conformal interface with wrinkled skin and for low-motion artifact in bio-potential monitoring, 2) high air permeability (\approx 4107 g m⁻²d⁻¹) for suppressing skin allergies during prolonged use, 3) dynamic adhesion to prevent interfacial delamination enabled by subsurface pores to relieve the concentration of interfacial stress under dynamic motion, and (4) mild adhesion force (≈0.09N) for preventing iatrogenic skin injuries during removal from delicate skin. Unlike commercial gel electrodes, our platform not only exhibits consistent skin interfacial impedance but also acquires high-quality epidermal electrophysiological signals during prolonged skin attachment under deformation. Absence of additional modifications on skin interfacial adhesion results in low peel-off force of the electrode with the potential use on delicate skin. We compare the present work with previous studies in Table S1 (Supporting Information), providing a detailed comparison of key performance parameters - including impedance, breathability, signal quality (motion artifact and SNR), and adhesion. This comparison highlights the competitive performance of our all-dry epidermal electrodes among state-ofthe-art dry electrodes, demonstrating a well-balanced performance across critical metrics: low impedance, high breathability, minimal motion artifact even under bending or stretching, acceptable SNR, and low adhesion. More importantly, our work is a demonstration of long-term monitoring using selfadhesive, all-dry electrodes for over 24 h without any additional tape.

2. Fabrication of All-Dry Epidermal Electrode (S-Porous Electrode)

Figure 1a illustrates S-porous electrodes including a top lowmodulus porous silicone elastomer layer and a bottom porous conductive carbon-doped silicone elastomer layer that possesses the octopus-like microstructures with a low density, and the interconnected pore networks with the subsurface porous structures. The effective arrangements of pore networks not only reduce effective elastic modulus to satisfy mechanical compliance with skin, [39,40] but also ensure breathability. [22,23,40] The gap between the subsurface pores and the electrode-skin interface plays an important role in effectively suppressing interfacial stress at the electrode edges during skin stretching, thereby preventing electrode delamination. Although our epidermal electrodes have ultrathin planar portion (i.e., gap) less than 10 µm due to the subsurface pore microstructures, it does not significantly sacrifice breathability. The SEM image in Figure 1b shows the conformal attachment of the S-porous electrode over the wrinkled soft skin with no additional modifications on skin interfacial adhesion, indicating the excellent mechanical compliance with skin. In addition, the subsurface porous structures in the epidermal electrodes are formed on the purpose of diminishing the interfacial stress concentration during skin deformation, thereby suppressing the delamination of the electrode from skin, while not sacrificing the skin contact areas. Our S-porous electrode shows superior dynamic contacting behavior on top of a phantom skin dogbone upon stretching to the non-porous electrode and the entire porous (E-porous) electrode (Figure 1c-e; Figures S1 and S2 and Movie \$1, Supporting Information). Although our all-dry epidermal electrodes do not exhibit strong adhesion, they are capable of maintaining dynamic contact by suppressing delamination on dynamic deformable skin - a functionality enabled by the subsurface pores within the electrodes. The dynamic contacting behavior demonstrates the intact interface between the electrode and a soft elastomeric dog-bone. As the phantom skin dog-bone, on which the electrode is attached, is stretched at a constant speed, delamination of the electrode from the dog-bone occurs, accompanying a sharp decrease in tensile force. When stretching at a speed of 10 mm sec⁻¹ (25% strain sec⁻¹), the non-porous and the E-porous electrodes are delaminated from the phantom skin around $\approx 50\%$ strain due to the stress concentration at the interface, while the S-porous electrodes remain intact. Absence of additional modifications on skin interfacial adhesion induces mild adhesion to favor safe-and-easy removal of the S-porous electrodes from delicate skin (Figure 1f-h). Notably, unlike commercial neonatal intensive care unit (NICU) adhesive, the adhesion properties of the S-porous electrodes are maintained unchanged even after 24 h (Figure 1h).

S-porous electrodes using soft silicone elastomer (Ecoflex) are fabricated by using two-step water steam etching method (Figure 1i; Figure S3, Supporting Information). First, the bottom porous conductive carbon-doped silicone elastomer layer is fabricated by forming the pore networks with subsurface pore structures in the liquid-state, conductive carbon-doped silicone elastomer using a water steam etching process. To form the octopus-like pores underneath the

16136829, 0, Downloaded from https://onlinelibrary.wiley.com/doi/10.1002/smll.202507416 by Chi Hwan Lee - Purdue University (West Lafayette), Wiley Online Library on [26/10/2025]. See the Terms

conditions) on Wiley Online Library for rules of use; OA articles are governed by the applicable Creative Commons License

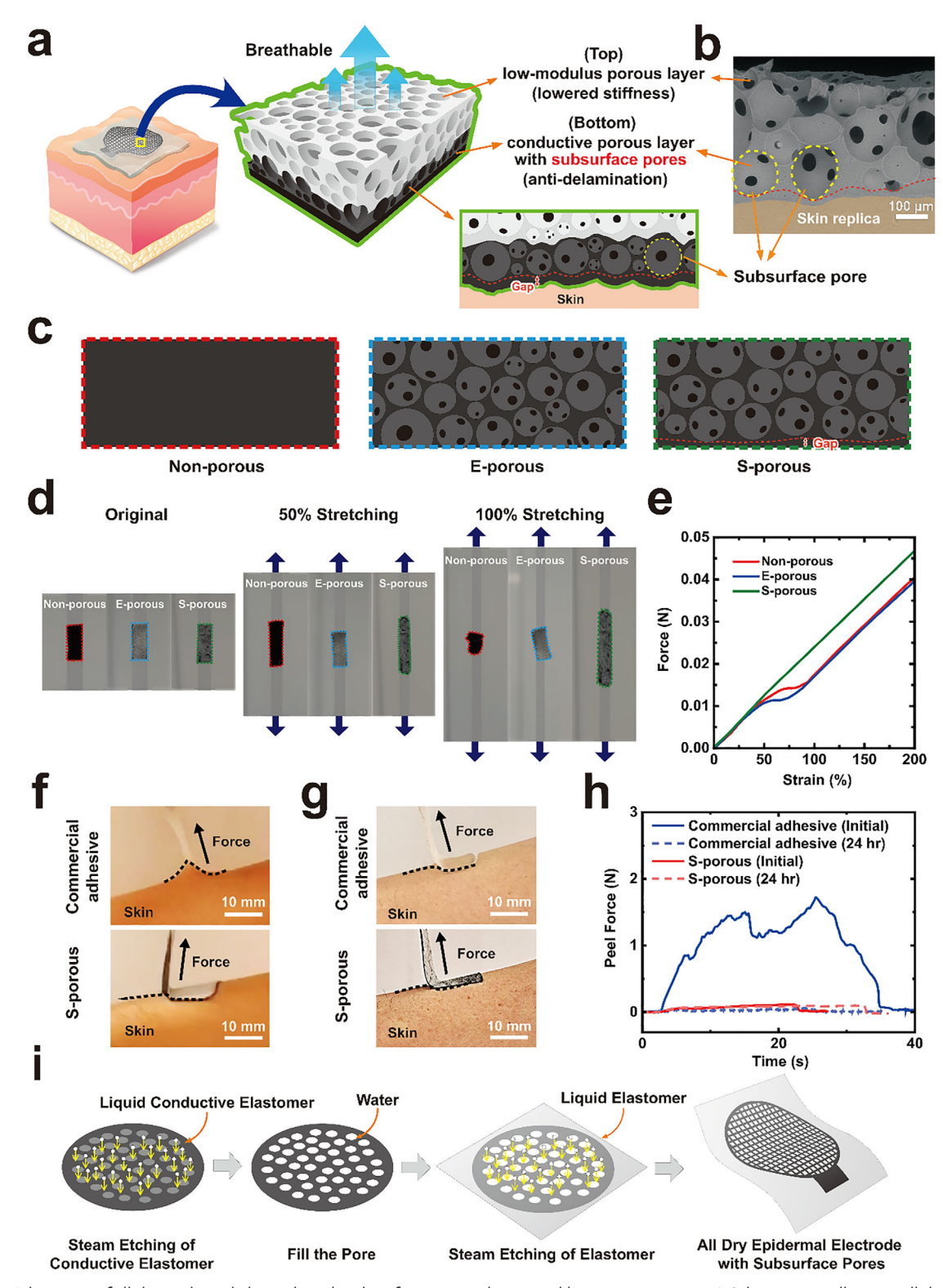


Figure 1. Fabrication of all-dry epidermal electrode with subsurface pore and octopus-like microstructures. a) Schematics to illustrate all-dry epidermal electrodes with subsurface pores and octopus-like microstructures. b) Cross-sectional SEM image of all-dry epidermal electrode attached onto skin replica. c) Schematics to illustrate the cross-sectional views of the non-porous, entire porous (E-porous), and subsurface porous (S-porous) epidermal electrodes. d) Optical images of non-porous, E-porous, S-porous electrodes attached on phantom skin dog-bone upon stretching by 0%, 50%, and 100%. e) Force-strain curves of non-porous, E-porous, S-porous electrodes attached on phantom skin dog-bone. Optical images to show peel-off behaviors of the commercial adhesive and the S-porous epidermal electrodes from the skin of a healthy adult after f) 0 and g) 24 h. h) Peel force curves of the commercial adhesive and the S-porous epidermal electrodes during removal from skin. i) Schematics to show fabrication processes of S-porous epidermal electrode.

16136829, D. Dowlookaded from https://onlinibithary.wiley.com/oi/01/01/02/smll.2029/146 by Chi Hwan Lee - Purtuse University (West Lafayetet), Wiley Online Library on [261012025]. See the Terms and Conditions (https://onlinelibitrary.wiley.com/terms-and-conditions) on Wiley Online Library for rules of use; OA articles are governed by the applicable Creative Commons Licensea

www.small-journal.com

bottom layer, the liquid-state, conductive carbon-doped silicone elastomer is screen-printed on the ceramic substrate capable of absorbing water that is vaporized and diffused out to the interface between the liquid-state elastomer and the ceramic substrate during the water steam etching process. To control the distance between the subsurface pore and the bottom surface of the electrode, the thickness of the screen-printed elastomer can be adjusted in consideration of the steam etching rate. The distance typically ranges up to ≈25 µm, with an average value of ≈10 µm. Then, the top low-modulus porous silicone elastomer layer is integrated over the bottom porous conductive carbon-doped silicone elastomer layer. To ensure the opening of the pore channels, it is important to prevent infiltration of the liquid-phase silicone elastomer mixture into the bottom porous layer during the second step of water steam etching. To achieve this, water is first infiltrated into the bottom porous layer, followed by the spin-coating of the liquid-phase silicone elastomer mixture, and the sample is then frozen at −20 °C for 2 h. Subsequently, the second water steam etching process is carried out. The detailed fabrication procedure is described in Experimental Section. To ensure interconnected pore networks, a cross-linking retarder is added to liquid-state soft silicone elastomer (Figure S4, Supporting Information). The silicone elastomer (Ecoflex) used in this study exhibits a fast curing rate. Therefore, without the addition of a curing rate retarder, the water steam etching process cannot produce a porous structure. The optimal conditions for generating pores are investigated by varying the amount of curing rate retarder. Pore depth and corresponding effective modulus are controlled in terms of volume fraction of cross-linking retarder in liquid-state silicone elastomer (Figure \$5, Supporting Information). The successful fabrication of S-porous electrodes shows negligible hysteresis upon the repeated stretching and releasing cyclic tests at 100% strain (Figure S6 and S7, Supporting Information). In addition, utilizing the water-absorbing ceramic substrate enables to form the low density (5%-13% of pore areas in bottom surface areas) octopus-like microstructures on the bottom surface of the conductive carbon-doped silicone elastomer layer during the first water steam etching. Specifically, the absorbed water in the ceramic substrate is diffused out to the interface between the liquid-state conductive carbon-doped silicone elastomer and the ceramic substrate, thereby generating the low-density, octopus-like microstructures (Figure S8, Supporting Information). Controlling the absorbed water contents (5-15 g) in the ceramic substrates determines the density of the octopus-like microstructures on the bottom surface (5%-13%) (Figure S8, Supporting Information).

3. Anti-Delaminating, Mechano-Electrical, and **Breathable Properties of S-Porous Electrodes**

Low-density, octopus-like microstructures on the bottom surface of S-porous electrodes assist the initial attachment of the electrode on the skin upon exerted pressure. It should be noted that the reasonably increased adhesion by controlling the density of octopus-like microstructures is important to the self-adhesive with mild adhesion. Octopus-like microstructures, which distribute on-surface shrinkable volume under external load, were reported to alter the normal and shear adhesion by 10%-300% range under dry conditions depending on the geometric parameters.[35,41,42] Low-density, octopus-like microstructures in this study represent 24%-30% increase in peel force, compared to the control samples with no octopus-like microstructures (Figure S9, Supporting Information), which is reasonably considered as the contribution of normal force generated by the pressure change. We further compare the changes in adhesion and interfacial toughness of S-porous electrodes to those of hydrogel-based commercial adhesive for 24 h (Figure \$10, Supporting Information). While the adhesion and interfacial toughness of the commercial adhesive greatly decreases after 24 h, our S-porous electrodes retain the initial adhesion and interfacial toughness.

The subsurface pores in the all-dry epidermal electrode (Figure 1a,b) serve to prevent delamination. Anti-delaminating properties of S-porous electrodes attached onto skins originate from the effective suppression of interfacial stress at the edges of the electrodes upon skin stretching by 100% (Figure 2a; Figure S11, Supporting Information). Particularly, the interfacial von Mises stress at the edge of the S-porous electrode is significantly reduced, compared to the non-porous electrode by up to a factor of 4.5. Stretching of skin changes the interfacial normal and shear stress distribution of the electrode adhering to the skin, inducing the interfacial stress concentration near the electrode edges.[43,44] When the interfacial shear stress exceeds the limit of interlaminar shear strength, edge delamination is initiated. [45–47] Upon stretching, the subsurface pores of S-porous electrodes are susceptible to large deformation, increasing the interfacial strain and stress underneath the subsurface pore, which effectively suppresses the sharp increase of the interfacial strain and stress near the edge (Figures S12 and S13, Supporting Information). Similar trend is observed for the simulation on S-porous electrodes with multiple pores (Figures S14 and S15, Supporting Information). When the distance between the subsurface pore and the interface decreases, the reduction of the interfacial normal and shear stresses at the edge becomes more distinct (Figure 2b,c; Figures S16 and S17, Supporting Information). The fabricated Sporous electrodes possess the subsurface pores with a distance of less than 10 µm from skin interface, playing an important role of their anti-delaminating properties.

The mechano-electrical properties of the porous conductive layer are tunable by controlling the doping ratio of conductive filler (i.e., carbon black particles) (Figure 2d; Figures S18 and S19, Supporting Information). As the contents of conductive filler increase, the electrical resistance of the porous conductive layer decreases, while the effective elastic modulus increases due to the relatively high stiffness of the conductive filler. Forming the pore and the conductive filler networks within the porous conductive layer achieves a low effective elastic modulus of 100 kPa with an electrical resistance of 5 k Ω upon the addition of 10 wt.% conductive filler. Further studies are carried out with S-porous electrodes, where the porous conductive layer with 10 wt.% conductive filler is deployed, to secure low skin interfacial impedance. Figure 2e,f shows the representative mechano-electrical properties of the S-porous electrodes, compared to non-porous electrodes. Notably, the S-porous electrodes, which include a top low modulus layer and a bottom conductive layer, exhibit a significantly low effective elastic modulus (16-19 kPa), demonstrating

16136829, 0, Downloaded from https://onlinelibrary.wiley.com/doi/10.1002/smll.202507416 by Chi Hwan Lee - Purdue University (West Lafayette), Wiley Online Library on [26/10/2025]. See the Terms

on Wiley Online Library for rules of use; OA articles are governed by the applicable Creative Commons License

www.small-journal.com

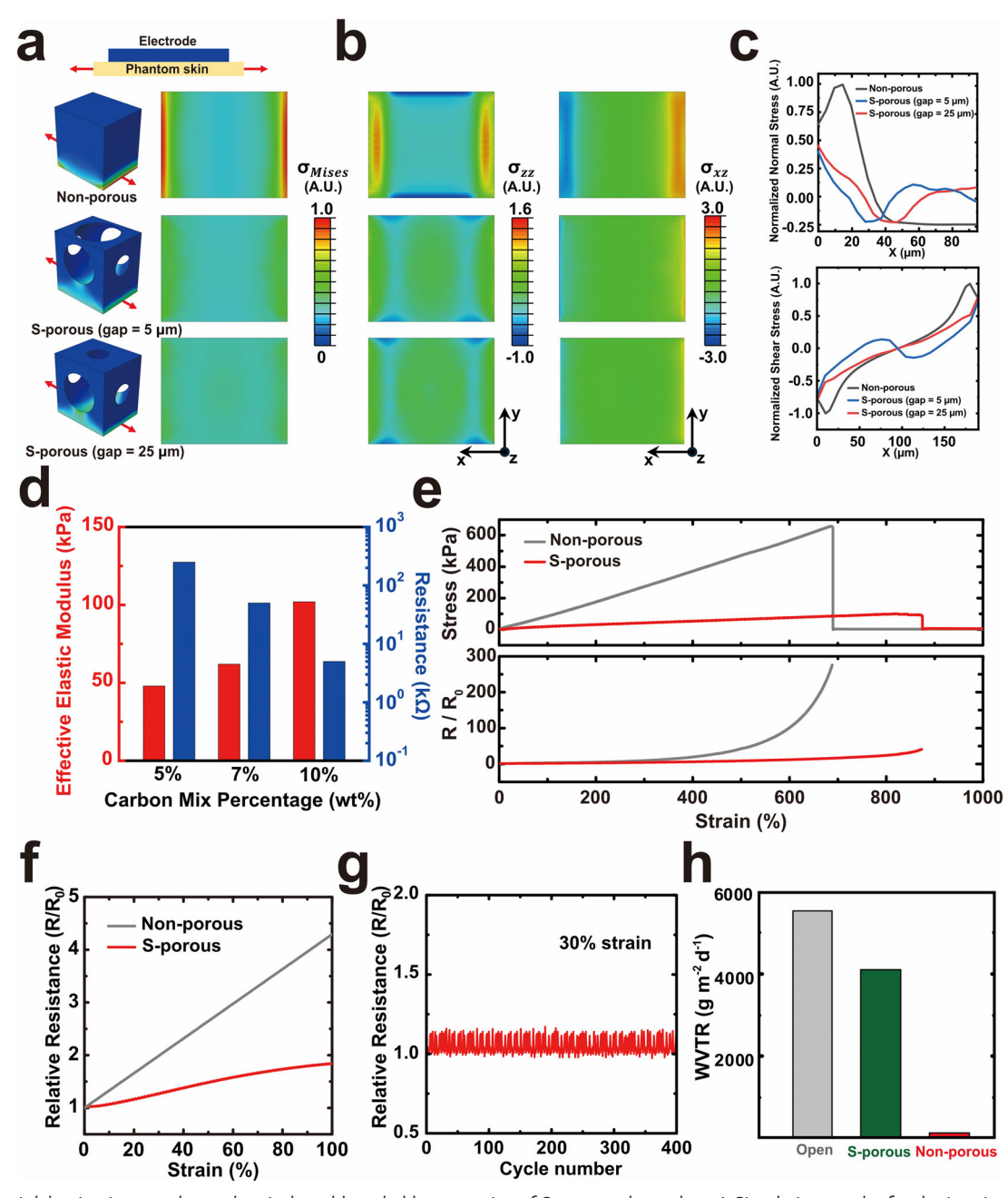


Figure 2. Anti-delaminating, mechano-electrical, and breathable properties of S-porous electrodes. a) Simulation results for the interior stress distribution of epidermal electrodes and interfacial stress of epidermal electrodes on phantom skins, b) Contours of interfacial normal and shear stresses of non-porous and S-porous electrodes. S-porous electrodes have 5 and 25 μ m distances between the subsurface pore and interface, respectively. c) Normalized normal and shear stress profiles at the interface of non-porous and S-porous electrodes in terms of x-axis. S-porous electrodes have 5 and 25 μ m distances between the subsurface pore and interface, respectively. d) Effective elastic modulus and electrical resistances of porous conductive layers with respect to different carbon-doping ratios (sample size (n) = 3). e) Stress–strain (top) and relative resistance (bottom) curves of non-porous and S-porous electrodes. Both are 10 wt.% carbon-doped. f) Relative resistance curves of non-porous and S-porous electrodes (10 wt.% carbon-doped) until 100% strain. g) Variations of the relative resistance of an S-porous electrode (10 wt.% carbon-doped) upon 400 repeated stretching and releasing cycles. h) Experimental results of air permeability (sample size (n) = 3).

their superior mechanical compliance for soft skin regions (e.g., anterior wrist, eyelid). Although S-porous electrodes have a relatively high thickness, their low effective elastic modulus enables low bending stiffness similar with epidermis. [48] Hence, our S-porous electrodes cannot only benefit easy handling, but also re-

alize conformal attachment to wrinkled soft skin. In addition, the S-porous electrode shows excellent mechano-electrical stability with little change (≈80% change in 100% strain) in relative electrical resistance. The considerably reduced changes in the relative electrical resistance are attributed to the maintained conductive

16136829, 0, Downloaded from https://onlinelibrary.wiley.com/doi/10.1002/sml1.202507416 by Chi Hwan Lee - Purdue University (West Lafayette), Wiley Online Library on [26/10/2025]. See the Terms

-conditions) on Wiley Online Library for rules of use; OA articles are governed by the applicable Creative Commons License

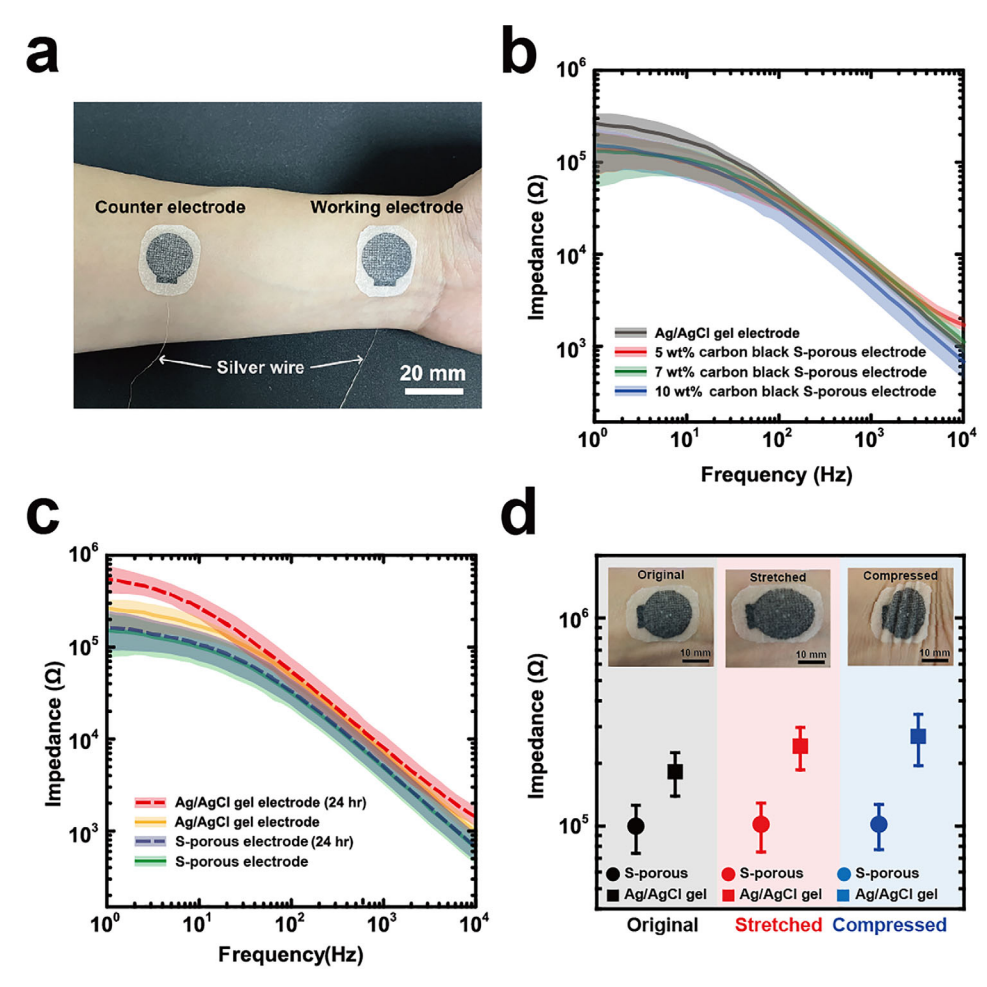


Figure 3. Skin interfacial impedance of S-porous epidermal electrode. a) Measurement configuration of skin interfacial impedance, b) skin interfacial impedance of commercial Ag/AgCl gel electrodes and S-porous epidermal electrodes with 5, 7, and 10 wt.% carbon doping. c) Skin interfacial impedance spectra of S-porous epidermal electrode (10 wt.% carbon-doped) and commercial Ag/AgCl gel electrode (initial and after 24 h). d) Skin interfacial impedance change of commercial Ag/AgCl gel electrode and S-porous epidermal electrode (10 wt.% carbon-doped) under skin deformation (Frequency = 10 Hz). (b–d) Sample size (n) = 5.

channels by pore deformation.^[39,49] Moreover, the variation of the relative electrical resistance is stably maintained within 15% during the repeated 400 stretching and releasing cycles (Figure 2g). Minimal change in electrical resistance upon stretching can benefit the accurate and stable acquisition of electrophysiological signals in daily life. To demonstrate the breathability of our Sporous path, an air permeability test is performed according to ASTM E96-95 (wet cup method) (Figure 2h). S-porous electrode shows excellent air permeability (4107 g m⁻²d⁻¹, 73% of open case) owing to the thin continuous layer (less than ≈10 µm) underneath the subsurface pores. Cell viability exceeding 90% for S-porous electrode in mammalian cell cytotoxicity tests after 24 and 48 h (Figure \$20, Supporting Information) also shows the biocompatibility of S-porous electrode. Lastly, to confirm the favorable safe-and-easy removal functionality of the S-porous electrodes from delicate skin, we conduct comparative removal tests of the electrodes after 24-hour attachment on the inner forearm using our S-porous electrodes and commercial adhesives. As shown in Figure S21 (Supporting Information), the commercial adhesives cause visible skin inflammation and redness after removal, while no such symptoms are observed with our S-porous electrode.

4. Low Skin Interfacial Impedance and Low-Motion Artifact Electrophysiological Signal Recording of S-Porous Epidermal Electrode

Long-term on-skin electrophysiological monitoring necessitates maintaining low skin interfacial impedance under skin deformation. This requires both high electrical conductivity of interfacial materials and good conformal contacts under dynamic conditions. To evaluate the skin interfacial impedance of our Sporous electrodes, a dual-electrode setup is used as shown in Figure 3a. S-porous electrodes with different carbon doping ratios show a low skin interfacial impedance to commercial Ag/AgCl gel electrodes in frequencies of 10 and 100 Hz (Figure 3b). Importantly, our S-porous electrodes have no additional modifications on skin interfacial adhesion. Compared to highly conductive interfacial materials, our S-porous electrodes

www.advancedsciencenews.com



16136829, 0. Dowloaded from https://oliniabeltamy.wile.com/doi/10.1002/smll.20250746 by Chi Hwa Lee - Purdue University (West Lafagette), Wiley Online Library on (261012025). See the Terms and Conditions (https://onlinebibrary.wiley.com/ems-and-conditions) on Wiley Online Library for rules of use; OA articles are governed by the applicable Creative Commons.

www.small-journal.com

have much lower electrical conductivity. Nevertheless, the conformal contacts between electrode and skin are mainly correlate with skin interfacial impedance. [50] leading to the excellent skin interfacial impedance of S-porous electrodes. To further evaluate the role of the low-density octopus-like microstructures, we compare the air permeability, resistance, and impedance of S-porous electrodes with and without these features. The air permeability (4107 \pm 9 g m⁻²·d) and resistance (5030 \pm 150 Ω) of the Sporous electrodes with low-density octopus-like microstructures are comparable to those of the electrodes without them (air permeability: 4046 \pm 25 g m⁻²·d; resistance: 5000 \pm 100 Ω). However, the S-porous electrodes with low-density octopus-like microstructures exhibit slightly lower impedance (100 \pm 26 k Ω at 10 Hz) than those without such microstructures (117 + 35 k Ω at 10 Hz), which can be attributed to the enhanced adhesion force provided by these structures. These results support that lowdensity octopus-like microstructures improve adhesion and corresponding electrical performance without compromising other key parameters. Wet hydrogel-based epidermal electrodes or epidermal electrodes with wet conductive hydrogel adhesives suffer from dehydration-associated degradation in skin interfacial impedance. Partial delamination occurs for commercial Ag/AgCl gel electrodes attached to the anterior wrist for 24 h due to dehydration of wet conductive hydrogel adhesives, which greatly increases their skin interfacial impedance (Figure 3c). In contrast, our all-dry S-porous electrodes have distinct benefits in maintaining low skin interfacial impedance with negligible changes for >24 h. Upon skin deformation, good mechanical compliance of our S-porous electrode also benefits to maintain low skin interfacial impedance (Figure 3d). Note that all-dry S-porous electrodes can be vulnerable to hydration at the interfaces due to sweating, yet superior breathability of S-porous electrodes can also suppress the hydration-related issues.

We investigate the electrophysiological recording performance of our S-porous electrodes by means of electrocardiography (ECG) and electrooculography (EOG) measurements on anterior wrist and eyelids, respectively (Figure 4; Figure S22, Supporting Information). Although commercial Ag/AgCl gel electrodes on soft anterior wrist skins with an elastic modulus of 10-12 kPa^[51] show high quality ECG signals with the signal-to-noise ratio (SNR) of 6 dB in the initial stages, their signals are greatly diminished after 24 h on attachment due to partial delamination upon the combined effects of the dehydration of skin interfacial adhesives and the wrist movements (i.e., wrist flexion and extension) (Figure 4a,b). In contrast, our S-porous electrodes with no additional interfacial modifications not only exhibit high quality ECG signals with the SNR of 8 dB, but also maintain signal acquisition with comparable quality in identical experimental conditions (Figure 4c,d). Stable acquisition of high quality signals from S-porous electrodes can be attributed to their conformal contacts with skin for prolonged testing. Another long-term electrophysiological monitoring under skin deformation is verified by EOG signal monitoring on eyelids which suffer from repetitive skin deformation (i.e., eyeball moving and blinking) (Figure 4e). While commercial Ag/AgCl gel electrodes are nearly delaminated and acquired EOG signals are greatly degraded after 4 h of testing (Figure 4f), S-porous electrodes maintain conformal contacts with eyelid skins to enable stable acquisition of EOG signals (Figure 4g).

5. Discussion

The findings suggest a pathway for all-dry epidermal electrodes that not only maintain conformal contact during skin deformation with no additional interfacial adhesives but also induce low peel-off forces from skin. Our all-dry epidermal electrode provides the design for mechanical compliance, breathability, dynamic adhesion, and safe-and-easy removal functionalities through the subsurface pores embedded in carbon-doped silicone elastomer. Two-step water steam etching is employed to monolithically integrate octopus-like and subsurface microstructures to S-porous epidermal electrodes including a bottom conductive layer and a top low modulus layer. Upon prolonged testing, S-porous electrodes on soft skins maintain superior mechanical compliance with skin and conformal contacts with skin, enabling the negligible changes of skin interfacial impedance and the capabilities to acquire high quality ECG and EOG signals from anterior wrists and eyelids, respectively. Breathability of our S-porous electrodes should be further optimized to suppress delamination associated with hydration at the interfaces, such as sweating. The resulting platform can be potentially usable for signal monitoring from delicate skins of immature and aging patients, allowing long-term bio-potential monitoring without iatrogenic skin injury during removal.

6. Experimental Section

Fabrication of All-Dry Subsurface Porous Epidermal Electrode: All-dry subsurface porous electrode with low density of octopus-like microstructures was fabricated by using two step water steam etching process. First, a mixture was prepared with soft silicone elastomer (a mixture of Ecoflex 00-30 and Ecoflex gel in 1:1 weight ratio, Smooth-On), curing rate retarder (Slo-Jo, Smooth-On) and carbon black particles (Vulcan XC-72) at a weight ratio of 7.65:1.35:1 by using a mixer (ARE-310, Thinky). The uncured conductive carbon-doped soft silicone elastomer for the bottom layer (a thickness of 100 µm) was screen printed on a ceramic substrate, following electrode designs. To control the distance between the subsurface pore and the bottom surface of the electrode, the thickness of the screen-printed elastomer was adjusted in consideration of the steam etching rate. Then, the screen-printed carbon-doped silicone elastomer on the ceramic substrate was frozen at -20 °C for 2 h, after which the water steam etching process was carried out to produce the subsurface porous structures in a pressurized vessel for 60 min at 120 °C and 110 kPa. In this process, the ceramic substrate was capable of absorbing water which was vaporized and diffused to the interface between the liquid-state carbon-doped silicone elastomer and the ceramic substrate, thereby forming the octopuslike microstructures underneath the bottom layer. Afterward, to construct the top layer (a thickness of 200 µm), soft silicone elastomer containing the curing rate retarder (a thickness of 100 µm) was spin coated onto the bottom carbon-doped silicone elastomer, where water was infiltrated, after which the sample was frozen at -20 °C for 2 h to ensure the opening of the pore channels. Then, the second water steam etching process was carried out for 30 min at 120 °C and 110 kPa, after which the sample was fully dried in a vacuum oven at 80 °C for 30 min. The non-porous samples were fabricated by curing the conductive carbon-doped soft silicone elastomer as the bottom layer with a thickness of 100 µm at 120 °C for 60 min in a vacuum environment, after which the soft silicone elastomer as the top layer with a thickness of 200 µm was spin coated and cured at 120 °C for 30 min in a vacuum environment. The entire-porous samples were identically fabricated to the subsurface porous electrode, except in the thickness of the bottom layer as 90 μm and the top layer as 180 μm .

Measurement of Electrode Adhesion: The adhesion of the all-dry subsurface porous electrode to human skin was evaluated and compared with

16136829, 0, Downloaded from https://onlinelibrary.wiley.com/doi/10.1002/smll.202507416 by Chi Hwan Lee - Purdue University (West Lafayette), Wiley Online Library on [26/10/2025]. See the Terms

und-conditions) on Wiley Online Library for rules of use; OA articles are governed by the applicable Creative Commons License

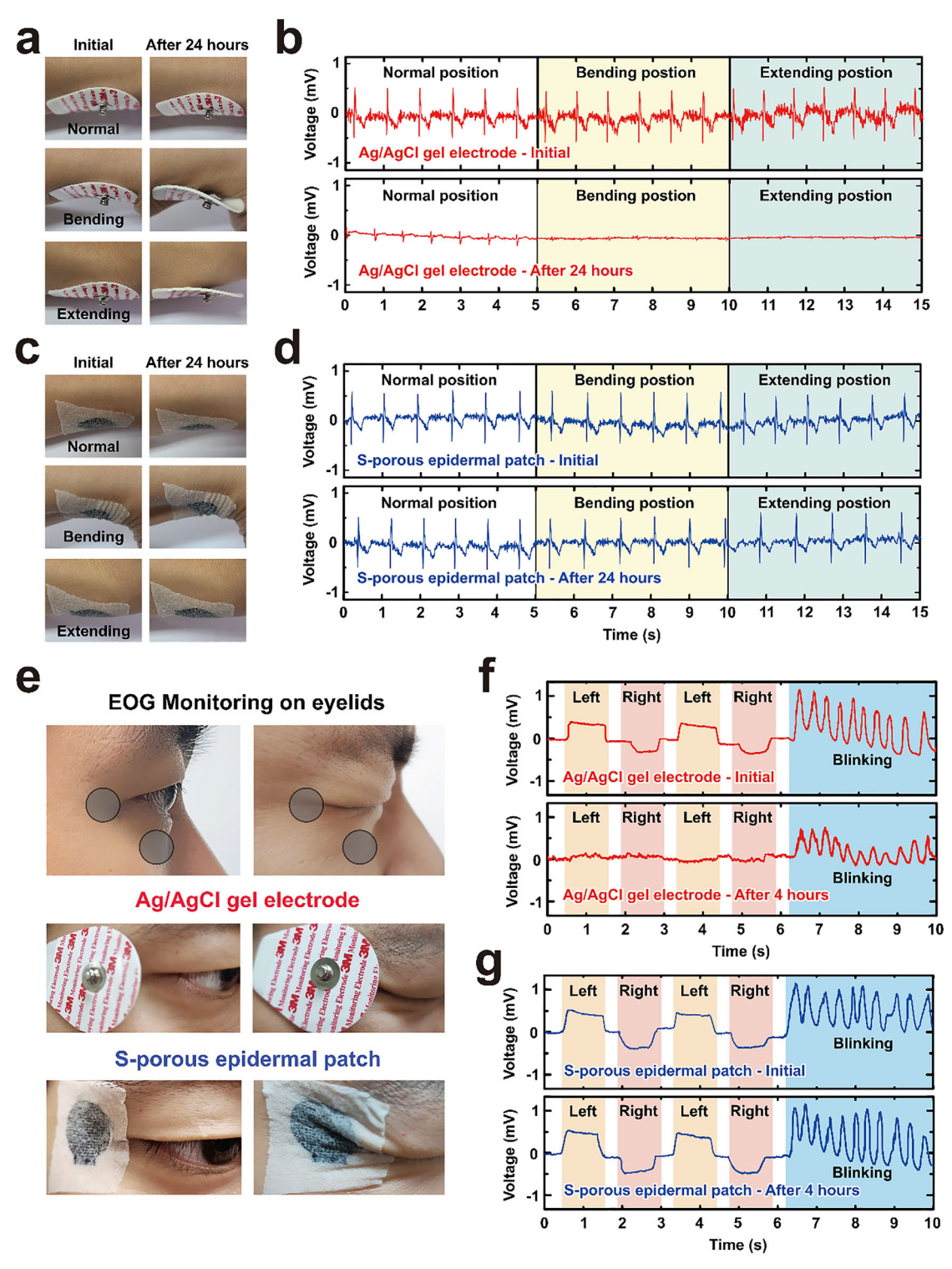


Figure 4. Low-motion artifact electrophysiological signal recording under skin deformation. a) Optical image and b) ECG signal recording of Ag/AgCl gel electrode attached on the anterior wrist, c) optical image and d) ECG signal recording of S-porous epidermal electrode attached on the anterior wrist, e) optical image of Ag/AgCl gel electrode and S-porous attached on the eyelids. EOG signal recording of f) Ag/AgCl gel electrode and g) S-porous epidermal electrode.

www.small-journal.com

that of commercial hydrogels (COVIDIEN Co., Ltd.). Adhesion tests were performed using a force gauge (Mark-10, USA) equipped with a 25 N load cell. A 90° peeling test was conducted at room temperature until complete detachment of the samples from the skin was achieved. The measured peeling force exhibited a plateau with slight oscillations as the peeling process reached a steady state. The interfacial toughness was calculated by dividing the plateau force by the width of the electrodes.

Measurement of Electrode Delamination for Substrate Stretching: A 100 μm thick ASTM-D412 dog-bone was fabricated by soft silicone elastomer (A mixture of Ecoflex 00–30 and Ecoflex gel in 1:1 weight ratio, Smooth-On) and 12 mm \times 6 mm sized epidermal electrode was attached to the middle part of dog-bone. The measurements of electrode delamination for phantom skin dogbone stretching were conducted using a universal testing machine (AG-10kNX Plus, Shimadzu). The load cell was 10 N, and the uniaxial strain was applied at a rate of 10 , 5 , and 0.5 mm sec $^{-1}$.

Cross-Linking Rate and Temperature Measurement: The cross-linking rate and temperature was measured by utilizing differential scanning calorimetry measurement (DSC, DSC-4000, Perkin Elmer) to demonstrate the modified cross-linking rates and temperatures of soft silicone elastomer and curing rate retarder mixtures. The pre-mixed soft silicone elastomers with and retarder of 0%, 5%, 10%, and 15% respectively were prepared with a total weight of 6–10 mg. The measured heat flows (W/g) and total heat of reaction (J/g) were normalized to the weight as following the temperature increase from 20 to 200 °C at a heating rate of 5 °C min $^{-1}$. After measuring the heat flow variation in terms of temperature, the cross-linking rate (s $^{-1}$) at each temperature point was calculated to divide peak heat flow (W/g) by total heat of reaction (J/g) as the following equation: $^{(52,53)}$

$$\alpha = \frac{\Delta H_T}{\Delta H_O} \tag{1}$$

where α is cross-linking rate (s⁻¹), ΔH_T is peak heat flow (W/g), and ΔH_O is total heat of reaction (J/g).

FEA Simulations of All-Dry Epidermal Electrode: The commercial software ABAQUS (ABAQUS 2023) was used to demonstrate mechanical behavior of the all-dry epidermal electrode (0.20 mm \times 0.16 mm \times 0.19 mm), which were attached on phantom skin (0.20 mm \times 0.16 mm \times 0.05 mm) and subjected to 100% stretching. The all-dry epidermal electrode and phantom skin were modeled by using hexahedron elements (C3D8R). For an interface stress analysis based on the distance between the pore and the interface, the overall size (0.20 mm \times 0.16 mm \times 0.19 mm) and the porosity (75%) of the subsurface porous epidermal electrode were fixed and the spherical pore shape was modified. All-dry epidermal electrode was modeled with the Ogden hyper elastic model using the tensile test results with a Poisson ratio of 0.45. Elastic modulus and Poisson ratio used for the phantom skin were 0.66 MPa and 0.45.

Mechano-Electrical Characterization: To measure the relative electrical resistance as a function of strain, carbon black doped soft silicone elastomers were connected with metal wires using Ag paste to enhance electrical contact between carbon black doped soft silicone elastomers and metal wires connecting to electrometer (Keithley 6514). Strain was applied by a universal testing machine (AG-10kNX Plus, Shimadzu).

Humid Air Permeability Measurement: Humid air permeability of alldry epidermal electrodes was measured by following ASTM E96-95 (wet cup method). All epidermal electrodes were fabricated of 16 cm² size to cover the top of small glass cylinder. Each glass cylinder (volume: 40 ml; diameter: 17 mm) contained 25 g of distilled water. All encapsulated jars were tested by measuring the mass variation in the environmental chamber at the temperature of 25 °C and the relative humidity of 40% for one week.

Cell Viability Test: The all-dry epidermal electrodes were sterilized with an ethanol-DI water mixture (70:30 v/v) for 30 min, rinsed with Dulbecco's phosphate buffered saline (PBS, Gibco), and dehydrated with UV irradiation for 1 h. The sterilized epidermal electrodes were then placed inside a 24-well plate. Rat cardiomyocyte cell (H9C2, ATCC) with the density of 1×10^5 /well was seeded into each well with a cell media (Dulbecco's Modified Eagle's Medium, ATCC) and subsequently incubated in a humid incu-

bator maintained at 37 °C with 5% CO_2 for 24 and 48 h. 200 μ L volume of 3-(4,5-dimethylthiazol-2-yl)-2,5-diphenyltetrazolium bromide (MTT, MilliporeSigma) reagent was added to each well and incubated for 3 h. Following removal of the cell media, cells were lysed with 400 μ L of dimethylsulfoxide (ATCC) per well. The absorbance of each well was measured using a microplate reader (Synergy NEO, BioTek) at a wavelength of 570 nm.

Skin Interfacial Impedance Measurement: The impedance recording experiments were carried out with the potentiostat (SP-200, Bio-Logic) with dual electrodes. Electrode settings can be seen in Figure 3a. The impedance spectra were recorded in the ranges of $1-10^4$ Hz. The area of each electrode used was 27 mm \times 20 mm, and the center-to-center distance between the two electrodes was 75 mm.

Electrophysiological Signal Sensing: Electrooculography (EOG) signals were acquired by using electrophysiological data acquisition unit (Power-Lab, ADInstruments) with bio-amplifier (Quad Bio Amp, ADInstruments). All EOG signals were filtered by a custom digital filter (high pass cutoff frequency: 50 Hz, low pass cutoff frequency: 30 Hz) near the eyelids. Signal-to-noise ratio (SNR) was calculated from the recorded ECG signals using the following formula,

SNR (dB) =
$$20 \cdot \log_{10}(\frac{A_{signal}}{A_{noise}})$$
 (2)

where SNR is signal-to-noise ratio (dB), A_{signal} is the amplitude of the signal, and A_{noise} is the amplitude of the noise. All the human studies were conducted in compliance with the university regulations and approved by Hanyang University Institutional Review Board (IRB protocol #: 202212-009-5). Informed written consent was obtained from all participants.

Statistical Analysis: All statistical analyses were conducted using Origin software (Origin Lab). Statistical significance was defined as P < 0.05. The sample sizes (n) were five for quantifying electrode adhesion and cross-linking rate. Electrode delamination and mechano-electrical characterization were carried out with n=3, and water vapor transmission rate (WVTR) was quantified with n=3. For the cell viability test, statistical analysis was performed using a one-way ANOVA with Tukey's post hoc test implemented in Origin software, and results were expressed as mean \pm s.e.m. (n=5). Skin impedance magnitudes at 10 and 100 Hz were extracted from Bode plots and compared across sample groups (n=5). Electrophysiological data acquired from the data acquisition unit were post-processed with LabChart software.

Supporting Information

Supporting Information is available from the Wiley Online Library or from the author.

Acknowledgements

M.S.J. acknowledges the support from Institute of Information & Communications Technology Planning & Evaluation (IITP) grant funded by the Korea Government (MSIT) (No.2020-0-01373, Artificial Intelligence Graduate School Program (Hanyang University)) and the research fund of Hanyang University (HY-202100000000667). D.R.K. acknowledges the support from Nano-Material Technology Development Program (NRF-2022M3H4A1A02046445) of the National Research Foundation of Korea (NRF), funded by the Ministry of Science and ICT of Korea. C.H.L acknowledges support from the Leslie A. Geddes Endowment and the Korea Institute for Advancement of Technology (KIAT) grant, funded by the Korea Government (MOTIE) (Global Industrial Technology Cooperation Center support program and International Cooperative R&D program (P0028319)).

Conflict of Interest

The authors declare no conflict of interest.

www.small-journal.com

16136829, 0, Downloaded from https://onlinelibrary.wiley.com/doi/10.1002/smll.202507416 by Chi Hwan Lee - Purdue University (West Lafayette), Wiley Online Library on [26/10/2025]. See the Terms

on Wiley Online Library for rules of use; OA articles are governed by the applicable Creative Commons

Author Contributions

M.S.J., J.Y., S.H., and J.L. contributed equally to this work. D.R.K. and C.H.L. conceived the concept; planned the project; and supervised the research. M.S.J, J.Y., S.H., J.L, H.J., B.K., H.L, C.H.L., and D.R.K. conducted experiments and data analysis on all-dry epidermal electrodes. M.S.J., J.Y., S.H., J.L., C.H.L., and D.R.K. wrote the manuscript. All authors commented on the paper.

Data Availability Statement

The data that support the findings of this study are available from the corresponding author upon reasonable request.

Keywords

electrophysiological monitoring, epidermal electrode, porous microstructure, soft material, wearable sensor

Received: July 19, 2025 Revised: October 9, 2025 Published online:

- [1] J. Shao, X. Li, Y. Li, J. Lin, P. Huang, Adv. Mater. 2024, 36, 2308217.
- [2] I. Hwang, H. N. Kim, M. Seong, S.-H. Lee, M. Kang, H. Yi, W. G. Bae, M. K. Kwak, H. E. Jeong, Adv. Healthcare Mater. 2018, 7, 1800275.
- [3] K. Zulkowski, Adv. Skin. Wound. Care. 2017, 30, 372.
- [4] Y. Wang, H. Haick, S. Guo, C. Wang, S. Lee, T. Yokota, T. Someya, Chem. Soc. Rev. 2022, 51, 3759.
- [5] K. Sim, F. Ershad, Y. Zhang, P. Yang, H. Shim, Z. Rao, Y. Lu, A. Thukral, A. Elgalad, Y. Xi, B. Tian, D. A. Taylor, C. Yu, Nat. Electron. 2020, 3, 775.
- [6] G. Choi, J. Kim, H. Kim, H. Bae, B.-J. Kim, H. J. Lee, H. Jang, M. Seong, S. M. Tawfik, J. J. Kim, H. E. Jeong, Adv. Mater. 2025, 37, 2412271.
- [7] S.-H. Sunwoo, S. I. Han, D. Jung, M. Kim, S. Nam, H. Lee, S. Choi, H. Kang, Y. S. Cho, D.-H. Yeom, M.-J. Cha, S. Lee, S.-P. Lee, T. Hyeon, D.-H. Kim, ACS Nano 2023, 17, 7550.
- [8] S. Patel, F. Ershad, J. Lee, L. Chacon-Alberty, Y. Wang, M. A. Morales-Garza, A. Haces-Garcia, S. Jang, L. Gonzalez, L. Contreras, A. Agarwal, Z. Rao, G. Liu, I. R. Efimov, Y. S. Zhang, M. Zhao, R. R. Isseroff, A. Karim, A. Elgalad, W. Zhu, X. Wu, C. Yu, Small 2022, 18, 2107099
- [9] M. Yuan, Y. Long, T. Liu, J. Liu, S. Qiu, T. Lin, F. Xu, Y. Fang, Mater. Today 2024, 75, 166.
- [10] L. Meng, Q. Fu, S. Hao, F. Xu, J. Yang, Chem. Eng. J. 2022, 427, 131999.
- [11] Y. Zhang, T. H. Tao, Adv. Mater. 2019, 31, 1905767.
- [12] C. Lim, Y. J. Hong, J. Jung, Y. Shin, S.-H. Sunwoo, S. Baik, O. K. Park, S. H. Choi, T. Hyeon, J. H. Kim, S. Lee, D.-H. Kim, Sci. Adv. 2021, 7, abd3716
- [13] S. Pan, F. Zhang, P. Cai, M. Wang, K. He, Y. Luo, Z. Li, G. Chen, S. Ji, Z. Liu, X. J. Loh, X. Chen, Adv. Funct. Mater. 2020, 30, 1909540.
- [14] S. H. Kim, S. Jung, I. S. Yoon, C. Lee, Y. Oh, J.-M. Hong, Adv. Mater. 2018, 30, 1800109.
- [15] Z. Zhang, J. Yang, H. Wang, C. Wang, Y. Gu, Y. Xu, S. Lee, T. Yokota, H. Haick, T. Someya, Y. Wang, Sci. Adv. 2024, 10, adj5389.
- [16] Q. Li, G. Chen, Y. Cui, S. Ji, Z. Liu, C. Wan, Y. Liu, Y. Lu, C. Wang, N. Zhang, Y. Cheng, K.-Q. Zhang, X. Chen, ACS Nano 2021, 15, 9955.
- [17] S. S. Kwak, S. Yoo, R. Avila, H. Chung, H. Jeong, C. Liu, J. L. Vogl, J. Kim, H.-J. Yoon, Y. Park, H. Ryu, G. Lee, J. Kim, J. Koo, Y. S. Oh, S. Kim, S. Xu, Z. Zhao, Z. Xie, Y. Huang, J. A. Rogers, Adv. Mater. 2021, 33, 2103974.
- [18] H. U. Chung, B. H. Kim, J. Y. Lee, J. Lee, Z. Xie, E. M. Ibler, K. Lee, A. Banks, J. Y. Jeong, J. Kim, C. Ogle, D. Grande, Y. Yu, H. Jang, P.

- Assem, D. Ryu, J. W. Kwak, M. Namkoong, J. B. Park, Y. Lee, D. H. Kim, A. Ryu, J. Jeong, K. You, B. Ji, Z. Liu, Q. Huo, X. Feng, Y. Deng, Y. Xu, et al., *Science* **2019**, *363*, aau0780.
- [19] S. Kim, B. Lee, J. T. Reeder, S. H. Seo, S.-U. Lee, A. Hourlier-Fargette, J. Shin, Y. Sekine, H. Jeong, Y. S. Oh, A. J. Aranyosi, S. P. Lee, J. B. Model, G. Lee, M.-H. Seo, S. S. Kwak, S. Jo, G. Park, S. Han, I. Park, H.-I. Jung, R. Ghaffari, J. Koo, P. V. Braun, J. A. Rogers, *Proc. Natl. Acad. Sci. USA* 2020, 117, 27906.
- [20] K. R. Jinkins, S. Li, H. Arafa, H. Jeong, Y. J. Lee, C. Wu, E. Campisi, X. Ni, D. Cho, Y. Huang, J. A. Rogers, Sci. Adv. 2022, 8, abo0537.
- [21] W. Liu, R. Xie, J. Zhu, J. Wu, J. Hui, X. Zheng, F. Huo, D. Fan, npj Flexible Electron. 2022, 6, 68.
- [22] W. Zhou, S. Yao, H. Wang, Q. Du, Y. Ma, Y. Zhu, ACS Nano 2020, 14, 5798.
- [23] Y. Liu, Y. Cheng, L. Shi, R. Wang, J. Sun, ACS Appl. Mater. Interfaces 2022, 14, 12812.
- [24] L. Tang, S. Yang, K. Zhang, X. Jiang, Adv. Sci. 2022, 9, 2202043.
- [25] N. Matsuhisa, Y. Jiang, Z. Liu, G. Chen, C. Wan, Y. Kim, J. Kang, H. Tran, H.-C. Wu, I. You, Z. Bao, X. Chen, Adv. Electron. Mater. 2019, 5, 1900347.
- [26] H. Yeon, H. Lee, Y. Kim, D. Lee, Y. Lee, J.-S. Lee, J. Shin, C. Choi, J.-H. Kang, J. M. Suh, H. Kim, H. S. Kum, J. Lee, D. Kim, K. Ko, B. S. Ma, P. Lin, S. Han, S. Kim, S.-H. Bae, T.-S. Kim, M.-C. Park, Y.-C. Joo, E. Kim, J. Han, J. Kim, Sci. Adv. 2021, 7, abg8459.
- [27] B. H. Kim, J. Lee, S. M. Won, Z. Xie, J.-K. Chang, Y. Yu, Y. K. Cho, H. Jang, J. Y. Jeong, Y. Lee, A. Ryu, D. H. Kim, K. H. Lee, J. Y. Lee, F. Liu, X. Wang, Q. Huo, S. Min, D. Wu, B. Ji, A. Banks, J. Kim, N. Oh, H. M. Jin, S. Han, D. Kang, C. H. Lee, Y. M. Song, Y. Zhang, Y. Huang, et al., ACS Nano 2018, 12, 4164.
- [28] Y. Zhao, S. Zhang, T. Yu, Y. Zhang, G. Ye, H. Cui, C. He, W. Jiang, Y. Zhai, C. Lu, X. Gu, N. Liu, Nat. Commun. 2021, 12, 4880.
- [29] D. Qi, Z. Liu, Y. Liu, Y. Jiang, W. R. Leow, M. Pal, S. Pan, H. Yang, Y. Wang, X. Zhang, J. Yu, B. Li, Z. Yu, W. Wang, X. Chen, Adv. Mater. 2017, 29, 1702800.
- [30] L. Zhang, K. S. Kumar, H. He, C. J. Cai, X. He, H. Gao, S. Yue, C. Li, R. C.-S. Seet, H. Ren, J. Ouyang, *Nat. Commun.* 2020, 11, 4683.
- [31] X. Ye, L. Li, Z. Wang, Y. Wang, J. Yang, M. Zheng, M. Wang, Z. Ji, S. Lin, Y. Zhang, J. Luo, J. Yi, P. Zhou, X. Cao, X. He, Y. Wang, ACS Sens. 2025, 10, 6218.
- [32] A. Majumder, A. Ghatak, A. Sharma, Science 2007, 318, 258.
- [33] A. Ghareeb, A. Elbanna, J. Appl. Mech. 2018, 85, 121003.
- [34] H. Min, S. Baik, J. Kim, J. Lee, B.-G. Bok, J. H. Song, M.-S. Kim, C. Pang, Adv. Funct. Mater. 2022, 32, 2107285.
- [35] S. Baik, D. W. Kim, Y. Park, T.-J. Lee, S. Ho Bhang, C. Pang, *Nature* 2017, 546, 396.
- [36] S. Baik, H. J. Lee, D. W. Kim, H. Min, C. Pang, ACS Appl. Mater. Interfaces. 2019, 11, 25674.
- [37] D. W. Kim, S. Baik, H. Min, S. Chun, H. J. Lee, K. H. Kim, J. Y. Lee, C. Pang, Adv. Funct. Mater. 2019, 29, 1807614.
- [38] H. U. Chung, A. Y. Rwei, A. Hourlier-Fargette, S. Xu, K. Lee, E. C. Dunne, Z. Xie, C. Liu, A. Carlini, D. H. Kim, D. Ryu, E. Kulikova, J. Cao, I. C. Odland, K. B. Fields, B. Hopkins, A. Banks, C. Ogle, D. Grande, J. B. Park, J. Kim, M. Irie, H. Jang, J. Lee, Y. Park, J. Kim, H. H. Jo, H. Hahm, R. Avila, Y. Xu, et al., Nat. Med. 2020, 26, 418.
- [39] J. Park, S. Wang, M. Li, C. Ahn, J. K. Hyun, D. S. Kim, D. K. Kim, J. A. Rogers, Y. Huang, S. Jeon, *Nat. Commun.* 2012, 3, 916.
- [40] K.-I. Jang, S. Y. Han, S. Xu, K. E. Mathewson, Y. Zhang, J.-W. Jeong, G.-T. Kim, R. C. Webb, J. W. Lee, T. J. Dawidczyk, R. H. Kim, Y. M. Song, W.-H. Yeo, S. Kim, H. Cheng, S. I. Rhee, J. Chung, B. Kim, H. U. Chung, D. Lee, Y. Yang, M. Cho, J. G. Gaspar, R. Carbonari, M. Fabiani, G. Gratton, Y. Huang, J. A. Rogers, *Nat. Commun.* 2014, 5, 4779.
- [41] J. H. Song, S. Baik, D. W. Kim, T.-H. Yang, C. Pang, Chem. Eng. J. 2021, 423, 130194.

www.small-journal.com

16136829, 0, Downloaded from https://onlinelibrary

.wiley.com/doi/10.1002/smll.202507416 by Chi Hwan Lee - Purdue University (West Lafayette)

Wiley Online Library on [26/10/2025]. See the Terms

on Wiley Online Library for rules of use; OA articles are governed by the applicable Creative Commons

- [42] H. Min, S. Baik, J. Lee, D. W. Kim, J. H. Song, K. H. Kim, M.-S. Kim, C. Pang, Chem. Eng. J. 2022, 429, 132467.
- [43] J. T. Reeder, J. Choi, Y. Xue, P. Gutruf, J. Hanson, M. Liu, T. Ray, A. J. Bandodkar, R. Avila, W. Xia, S. Krishnan, S. Xu, K. Barnes, M. Pahnke, R. Ghaffari, Y. Huang, J. A. Rogers, Sci. Adv. 2019, 5, aau6356.
- [44] S. R. Krishnan, C.-J. Su, Z. Xie, M. Patel, S. R. Madhvapathy, Y. Xu, J. Freudman, B. Ng, S. Y. Heo, H. Wang, T. R. Ray, J. Leshock, I. Stankiewicz, X. Feng, Y. Huang, P. Gutruf, J. A. Rogers, Small 2018, *14*, 1803 192.
- [45] A. Ghatak, L. Mahadevan, J. Y. Chung, M. K. Chaudhury, V. Shenoy, Proc. R. Soc. Lond., Ser. A, Math. Phys. Eng. Sci. 2004, 460, 2725.
- [46] N. Tada, Y. Hu, T. Uemori, T. Nakata, MATEC Web Conf. 2017, 108, 01004.

- [47] C. T. Herakovich, J. Compos. Mater. 1981, 15, 336.
- [48] H. J. Shim, S.-H. Sunwoo, Y. Kim, J. H. Koo, D.-H. Kim, Adv. Healthcare. Mater. 2021, 10, 2002105.
- [49] J. Y. Oh, D. Lee, S. H. Hong, ACS Appl. Mater. Interfaces 2018, 10, 21666.
- [50] H. Wu, G. Yang, K. Zhu, S. Liu, W. Guo, Z. Jiang, Z. Li, Adv. Sci. 2021, 8, 2001938.
- [51] S. Park, J. Tao, L. Sun, C.-M. Fan, Y. Chen, Molecules 2019, 24, 907
- [52] R. N. Jana, G. B. Nando, J. Thermoplast. Compos. Mater. 2008, 21,
- [53] Z. Li, K. Hansen, Y. Yao, Y. Ma, K.-S. Moon, C. P. Wong, J. Mater. Chem. C 2013, 1, 4368.